Landslides (2005) 2: 221–228
DOI: 10.1007/s10346-005-0059-z
Received: 23 September 2004
Accepted: 6 May 2005
Published online: 16 July 2005

Lalan P. Singh · C. J. van Westen · P. K. Champati Ray · P. Pasquali

Accuracy assessment of InSAR derived input maps for landslide susceptibility analysis: a case study from the Swiss Alps

Abstract In recent years SAR interferometry has become a widely used technique for measuring altitude and displacement of the surface of the earth. Both these capabilities are highly relevant for landslide susceptibility studies. Although there are many problems that make the use of SAR interferometry less suitable for landslide inventory mapping, it's use in landslide monitoring and in the generation of input maps for landslide susceptibility assessment looks very promising. The present work attempts to evaluate the usefulness and limitations of this technique based on a case study in the Swiss Alps. Input maps were generated from ERS repeat pass data using SAR interferometry. A land cover map has been generated by image classification of multi-temporal SAR intensity images. An InSAR DEM was generated and a number of maps were derived from it, such as slope-, aspect, altitude- and slope form classes. These maps were used to generate landslide and rockfall susceptibility maps, which give fairly well acceptable results. However, a comparison of the InSAR DEM with the conventional Swisstopo DEM, indicated significant errors in the absolute height and slope angles derived from InSAR, especially along the ridges and in the valleys. These errors are caused by low coherence mostly due to layover and shadow effects. Visual comparison of stereo images created from hillshading maps and corresponding DEMs demonstrate that a considerable amount of topographic details have been lost in the InSAR-derived DEM. It is concluded that InSAR derived input maps are not ideal for landslide susceptibility assessment, but could be used if more accurate data is lacking.

Keywords Landslide susceptibility · InSAR · Digital elevation models

Introduction

As topography is one of the major factors in landslide hazard and risk analysis, the generation of a digital representation of the surface elevation, called Digital Elevation Model (DEM), plays a major role. During the last 15 years there have been important changes both in terms of data availability, as well as in terms of software that can be used on normal desktop computers, without extensive skills in photogrammetry. SAR interferometry is gaining increasing importance as a technique for rapid and accurate topographic data collection. Digital Elevation Models produced from this technique are becoming available, for example the general DEMs produced by the SRTM mission (Rabus et al. 2003). Synthetic Aperture Radar (SAR) images contain both the amplitude and phase information of the return signals from the earth surface. SAR interferometry (InSAR) is a technique in which two SAR images of the same portion of the earth taken from slightly different satellite positions are used (Massonnet and Feigl 1998; Rosen et al. 2000). Combining the two images results in an interferogram, which represents the phase difference between the return signals in the two SAR images, resulting from topography and from changes in the line-of-site distance (range) to the radar due to displacement of the surface or change in the propagation path length. The phase differences can be converted into a DEM if very precise satellite data are available. This technique can be applied for measuring displacements at the earth's surface with very high accuracy and for topographic mapping (Massonnet and Feigl 1998). A number of spaceborne InSAR systems are operational, (ERS, ENVISAT, RADARSAT) or in the planning and implementation stages and therefore it is important to understand the accuracy and limitations of the technique for different applications (Crosetto 2002).

The phase difference results from topography as well as due to displacement of the surface. Therefore, by separating the motion-related and the topography related phase contributions, mapping of landslide movements is possible. This can be done by the differential interferometry (DInSAR) technique using two interferograms of different time periods. In recent years this technique has been used to monitor and measure landslide movements (Fruneau et al. 1996; Rott et al. 1999; Kimura and Yamaguchi 2000; Rizo and Tesauro 2000; Squarzoni et al. 2003). The applicability of the DInSar method for detecting slope movements in vegetated terrain however is much less, due to phase decorrelation and atmospheric disturbances. Better results can be obtained by carrying out measurements on a subset of image pixels corresponding to pointwise stable reflectors (Permanent Scatterers, PS) and exploiting long temporal series of interferometric data, as demonstrated by Colesanti et al. (2003) with data from California and landslide areas near Ancona in Italy. The permanent scatterer method however, has the drawback that a large number of SAR scenes are required and that measurements can only be made for a limited number of points in the terrain. Radar interferometry has also been applied very successfully on the ground, as ground-based interferometry for the monitoring of landslides in Italy, as demonstrated by Tarchi et al. (2003), Antonello et al. (2004) and Pieraccini et al. (2003).

Methods and materials

In this paper we examine the usefulness of an InSAR derived DEM and intensity images generated from ERS repeat pass data for landslide susceptibility assessment. The findings presented in this paper are based on a case study in the Swiss Alps. The area is situated in south Switzerland, in the cantons of Fribourg and Bern (see Fig. 1). The landscape in the region is marked by glacial, hydrological and gravitational processes such as landslides and rockslides.

The following ERS data sets have been used:

- ERS tandem data of 7 and 8 November 1995,
- ERS tandem data of 22 and 23 October 1996,
- ERS–2 data of 5 April, 19 July, and 27 September 2000.

These data sets have been used to generate input maps for landslide susceptibility assessment, such as land cover, slope angle, slope aspect,

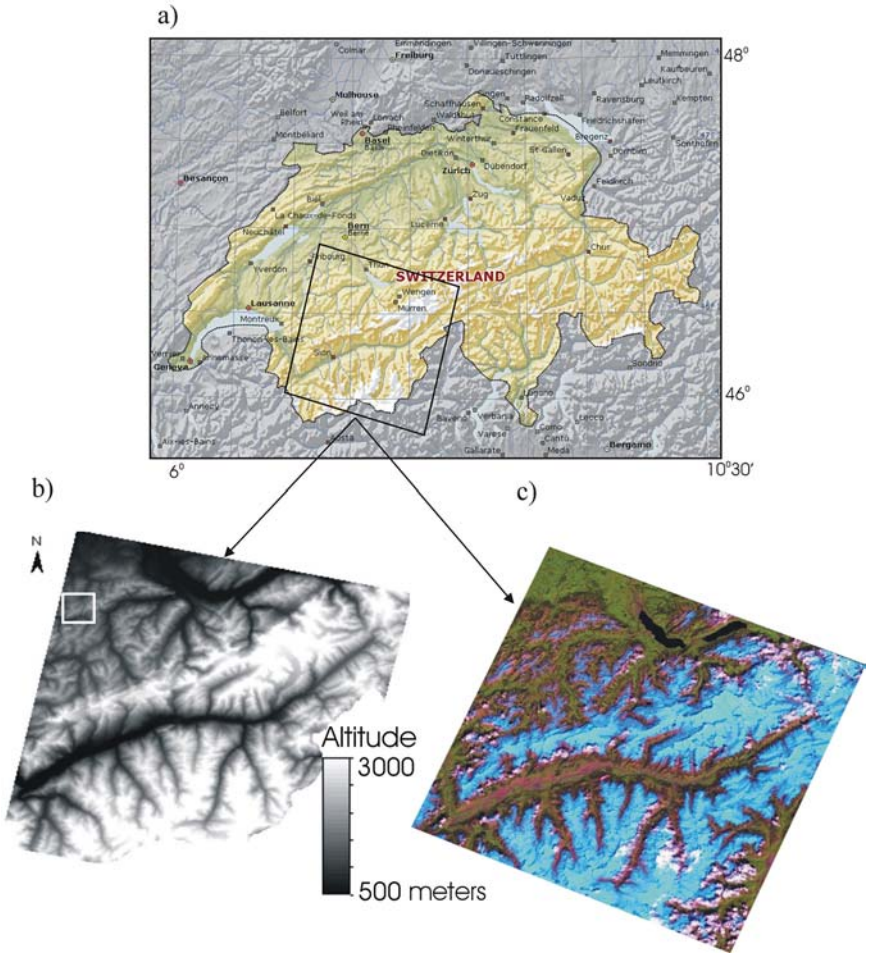

Fig. 1 Location map. **a**) Location of the ERS scenes within Switzerland; **b**) Hillshading image of the InSAR derived DEM, with the study area indicated as a *white box*; **c**) Landsat ETM image of the study area from 2002

slope form and relief. The data processing was done using SARscape software (Sarmap 2005). In the following sections the procedure is explained more in detail.

Extraction of a land cover map from multi-temporal intensity images

The different brightness levels in the Radar intensity images may help to differentiate the various terrain features and land cover types. If multi-temporal intensity images are available valuable information on land cover may be extracted as the brightness characteristics of different land cover types will change over time. For the present study the intensity images were generated from the three available ERS Single Look Complex (SLCs) data of 5 April, 19 July and 27 September 2000 using a focusing and multilooking operation of the SARscape software. All the intensity images were then co-registered and filtered for speckle removal using a time series filter. By applying this filter the full spatial resolution of the imagery is retained while there is a significant increase in the signal to noise ratio (SNR) (De Grandi et al. 1997). In this way, homogenous regions are optimally filtered while structural features are retained. These images were then geocoded and a False Colour Composite (FCC) was generated which shows a wide variability in terms of radar response of the region. In other words, it was possible to discriminate different landcover classes in the FCC. Training sites were selected from all the classes and the Jeffries-Matusita distance measure algorithm (Chips 2000) was used for determining the separability of the classes. It was observed that most of the classes were statistically separable. A Maximum Likelihood classification was performed with a standard deviation of 2 for the variability of each class. The resulting land cover map is shown in Fig. 2. About 24% of the land cover map could not be classified due to shadow (16%) and layover (8%). This effect could be reduced by using, when available, both ascending and descending acquisitions, minimizing therefore the percentage of unclassified pixels.

Generation of a DEM from InSAR

The InSAR DEM used for the present study was produced from ERS tandem data of 7/8 November 1995 and 22/23 October 1996. A combination of ascending and descending mode data were used, as this combination is essential for covering all slopes in the terrain (Pasquali et al. 1994). It is because the areas affected by foreshortening and layover in one image (e.g. ascending mode) are well covered (if not in shadow) in the other image (e.g. descending mode). The InSAR processing involved co-registration of the two tandem data sets, calculation of the interferometric phase and coherence, phase unwrapping and computation of the height. Since the phase unwrapping is the most crucial part of InSAR processing, involving reconstruction of phase to extract height information, any error committed at this stage affects the quality of the DEM. Various algorithms exist for unwrapping but no single one is sufficient. To overcome this problem a hybrid approach was implemented in the SARscape software, which is based on the fusion of a region-growing and an iteratively working

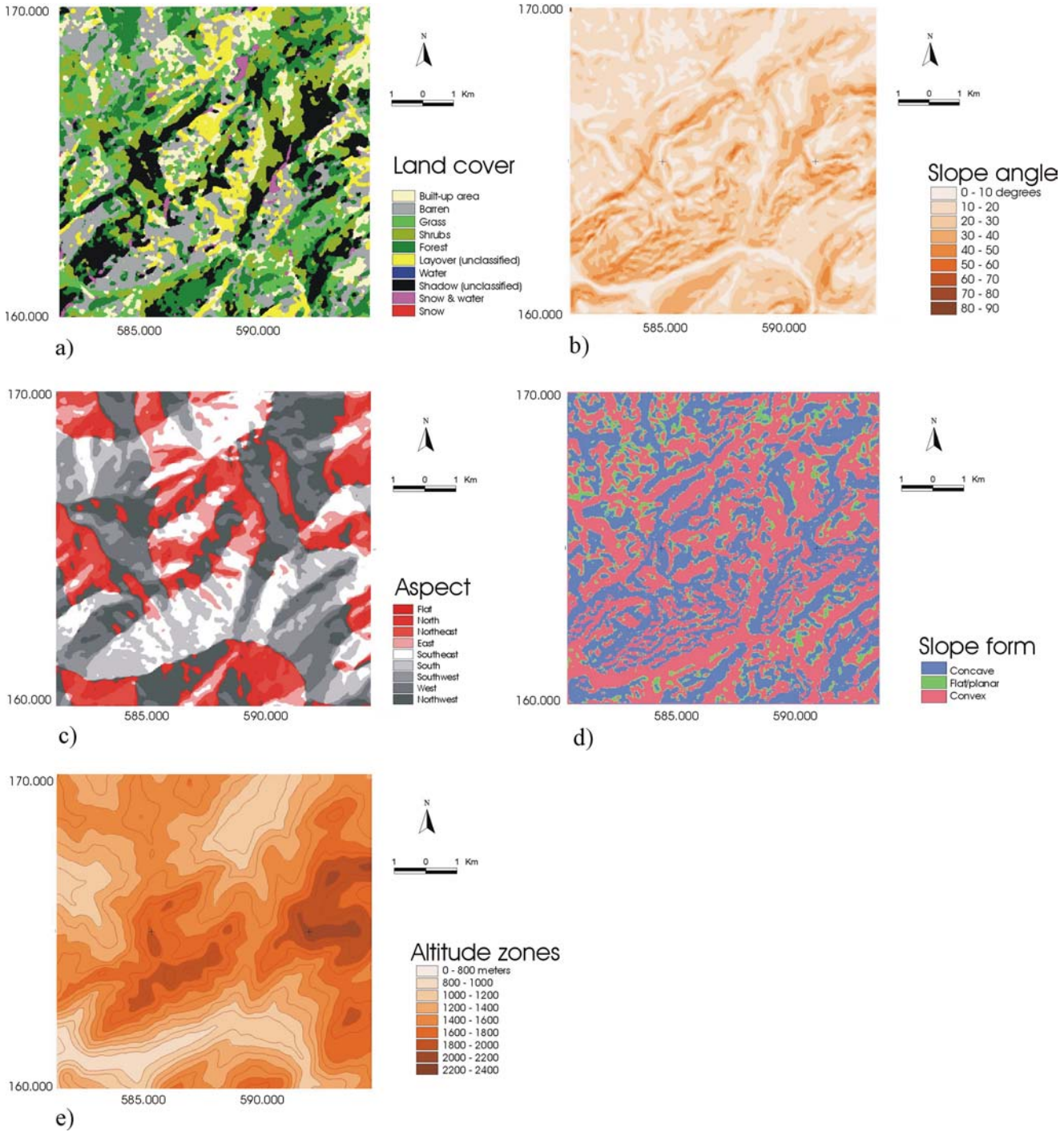

Fig. 2 Factor maps for landslide susceptibility derived from SAR (**a**) Land cover classes (**b**) Slope steepness classes (**c**) Slope aspect classes (**d**) Slope form classes (**e**) Altitude classes

2-D least square phase unwrapping algorithm (Reigber and Moreira 1997).

The unwrapped phase was converted into x, y, z Cartesian coordinates by employing range and Doppler approach using slant range, the Doppler and the interferometric equations (Holecz et al. 1998). The phase to height conversion implemented in the SARscape software is based on a rigorous approach and does not require an a-priori known DEM for the geocoding of the SAR-derived DEM (Holecz, personal communication). This approach is based on a fully three-dimensional model that connects the image space to object space. It uses observation equations that connect the image space (azimuth, slant range and interferometric phase) to the object space in the Cartesian system (Crosetto 2002). The procedure works pixel-wise and requires precise orbit knowledge of the two satellites (master and slave). However, the accuracy of the satellite orbits is usually not sufficient to achieve

an accurate DEM geocoding and therefore an InSAR geometry calibration with points of known height are needed. This was done by selecting GCPs from 1:25.000 and 1:50.000 Swiss topographic maps and converting them into slant range geometry. The points were selected from the part of the unwrapped image where coherence was good (more than 0.3 is preferred), where there are no problems in the unwrapping (e.g. not in areas that have a phase value very different from the surrounding region or discontinuities). The DEM was generated using a coherence threshold of 0.25. Interpolation was applied as the 3D points generated from interferometric phases are unevenly distributed because of two reasons (1) the slant range nature of SAR data makes the terrain sampling very irregular, (2) the phase of many interferogram pixels cannot be unwrapped: such pixels do not contribute to the grid generation, i.e. they result in "holes" in the grid (Crosetto 2002). The grid size of the DEM is 25 m. Several parameter maps for landslide susceptibility assessment, were generated from the DEM: altitude classes, slope steepness, slope aspect and slope form. The InSAR DEM was imported into the ILWIS 3.11 GIS software and various GIS modeling functionalities were used to generate the maps, which were later classified in a limited number of classes (See Fig. 2).

Statistical landslide susceptibility assessment using Insar derived parameter maps

The input maps generated from InSAR were used in a GIS to generate susceptibility maps for the two most prominent landslide types in the study area (i.e. shallow slides and rockfall) using the weights of evidence method (Bonham-Carter 1994; Van Westen 1993). In this method positive and negative weights (W_i^+ and W_i^-) are assigned to each of the different classes into which a factor map is classified (e.g. each lithological unit within a lithology map), and are defined as:

$$W_i^+ = \log_e \frac{P\{B_i|S\}}{P\{B_i|\bar{S}\}}$$

and

$$W_i^- = \log_e \frac{P\{\bar{B}_i|S\}}{P\{\bar{B}_i|\bar{S}\}}$$

where, B_i: presence of a potential landslide conditioning factor, $\bar{B}_i$: absence of a potential landslide conditioning factor, S: presence of a landslide, and $\bar{S}$: absence of a landslide.

For each factor, W_i^+ is used for those locations where a factor occurs (represented as a class in a multi-class map) to indicate the importance of the presence of the factor for the occurrence of landslides. If W_i^+ is positive the presence of the factor is favourable for the occurrence of landslides, and if W_i^+ is negative it is not favourable. W_i^- is used to evaluate the importance of the absence of the factor for the occurrence of landslides. When W_i^- is positive the absence of the factor is favourable for the occurrence of landslides. Weights with extreme values indicate that the factor is a useful one for the susceptibility mapping, while factors with a weight around zero have no relation with the occurrence of landslides.

Initiation areas for rockfall and shallow debris and soilslides were treated separately as these are two completely different phenomena governed by different terrain conditions. The landslide inventory map provided by the Swiss Federal Office for Water and Geology (FOWG) was used to develop the model and also for the validation of the results. The original inventory maps for the two processes are shown in Fig. 3b and c. The inventory maps show all features, of different ages, and including both the accumulation zone as well as the initiation zone. In order to carry out the analysis, only the active initiation zones were used, and both rock fall and shallow landslide datasets were randomly divided into two separate datasets; one for developing the model and one for validating the resulting susceptibility map.

The randomly selected map of the initiation areas was combined with the factor maps (e. g., land cover, slope, aspect, slope form and relief maps) through map overlaying in GIS, followed by the calculation of weights indicating the statistical relation of each class of the factor maps with the initiation zones. The individual factor maps were analyzed separately on the relative importance of the various map classes. For the rockfall initiation areas, the slopes falling in slope classes greater than 30° bear a positive relationship with the occurrence of rock fall. In the slope aspect map (Fig. 2c), it was observed that the north and northwest oriented slope classes have a positive correlation perhaps due to the fact that they are in shadow most of the time and experience more freezing activity leading to mechanical disintegration of rocks. In the slope form map (Fig. 2d), mostly the convex slopes are associated with rock fall. In the relief class map (Fig. 2e) the classes with an altitude of more than 1600 m. are associated with rockfalls.

The statistical relationship of the landslide map with the factor maps supports the assumption that shallow landslides occur under a different geoenvironmental setting than rockfalls in the region. In the land cover map, the classes such as grassland, dense vegetation and thinly vegetated areas, which mostly occur on more gentle slopes, show positive relation with the occurrence of landslides. In contrast, the classes having positive weights for rockfalls show a negative relation for shallow landslides. The weights for the slope aspect classes indicate that southwestern and western slopes experience more shallow slides. The slope curvature map indicates that concave slopes are mostly associated with landslides. In the relief map, the 1200–1400 m class and adjoining relief classes show a positive relationship with landslides.

After analyzing the final weights for all the classes in the different factor maps, the rock fall and shallow landslide susceptibility maps were generated and classified into five qualitative susceptibility classes (Fig. 3e and f) using cumulative histogram cut off values at 20%, 40%, 65%, and 85%. The resulting susceptibility maps were validated with the other half of the randomly selected initiation zones using the weights of evidence method (Van Westen 1993). The susceptibility classes show an overall good statistical validation, with negative weight values falling in very low susceptibility class and gradually becoming positive as one moves towards the higher susceptibility classes (see Tables 1 and 2).

Accuracy assessment of the INSAR DEM

In order to have a clearer idea of the reliability of InSAR derived DEM data for landslide susceptibility analysis, an accuracy assessment of the InSAR DEM product was attempted by comparing it with the Digital Elevation Model derived from the 1:25,000 Swiss Topographic Survey maps (DHM25). The DHM25 matrix model was derived by applying triangulation network interpolation to the basic model, which was extracted from the National Map (vectorized contours) of 1:25,000. The DHM25 has the same coordinate system and grid size as the InSAR DEM (Swiss Coordinate System and a grid size of 25 m). The average accuracy of the DHM25 with respect to photogrammetrically determined control points is about 3 m (Swisstopo 2002).

As the altitude values derived from InSAR provide a geometric altitude (i.e. height above a reference ellipsoid) while the altitude

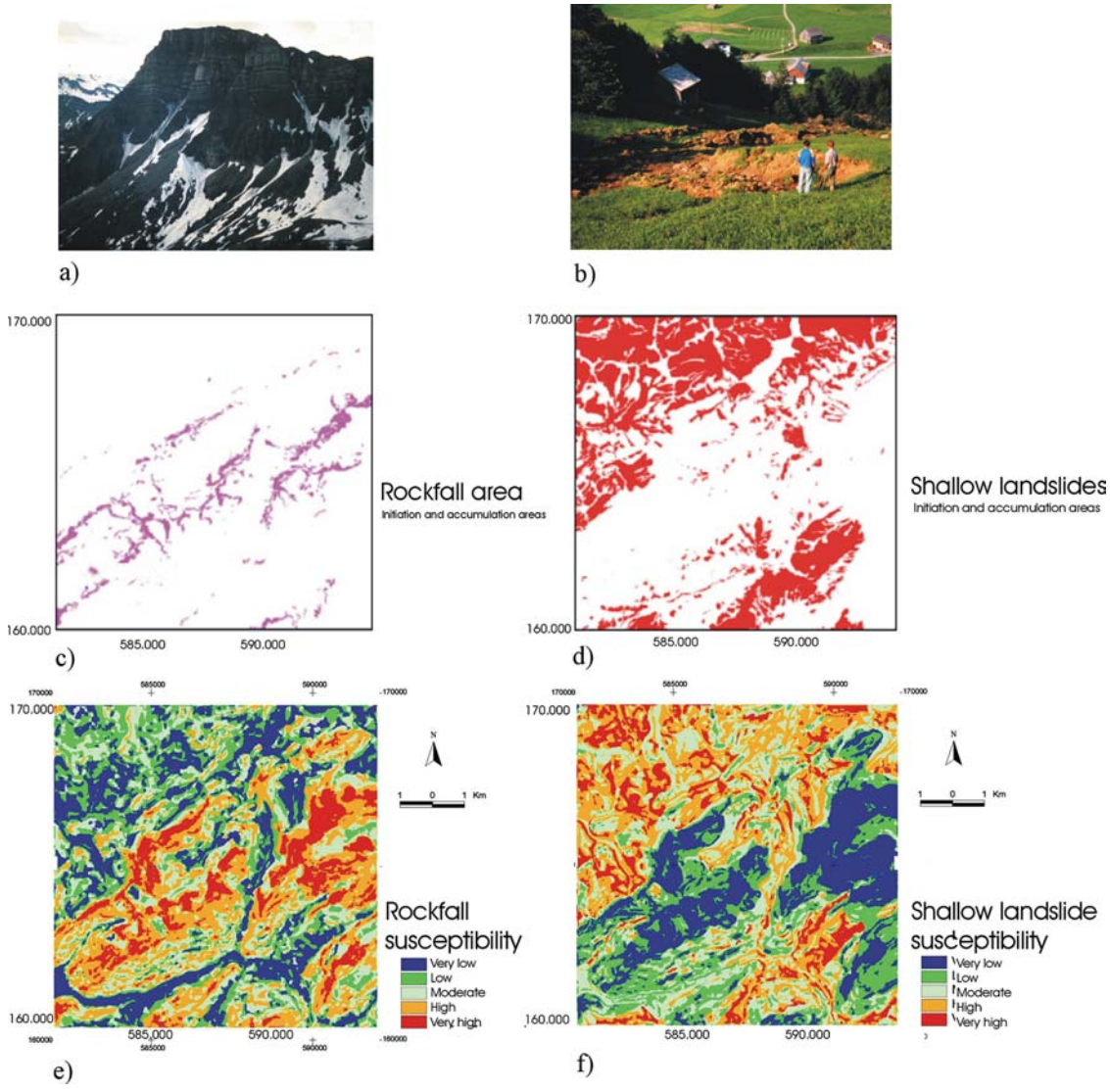

Fig. 3 (**a**) Typical rockfall zone in Alpine setting; (**b**) Characteristic shallow landslide in Alpine setting; (**c**) Rockfall inventory map, containing the rockfall initiation and accumulation areas, from the database collected by the Swiss Federal Office for Water and Geology (FOWG); (**d**) Inventory map of landslide features, containing all landslides from different periods from the FOWG database, excluding the rockfall features; (**e**) Rockfall susceptibility map generated using the Weights of Evidence Modeling as described in the text; (**f**) Shallow landslide susceptibility map, generated using the Weights of Evidence Modeling as described in the text

from DHM25 (derived from a topographic map) is a gravimetric altitude (i.e. height above mean sea level), it is often required to transform the datum before comparing the two DEMs (Gens and van Genderen 1996). In the present study, the datum transformation of the InSAR-derived DEM was performed considering the local geoidal undulations, to obtain a gravimetric height. For the height error estimation the InSAR DEM was subtracted from the DHM25 and an absolute elevation difference map was generated and reclassified into six difference classes (Fig. 4). Variation in height in the order of more than 50 m exists in about 8% of the map area and most of these

Table 1 Positive (W+), negative (W−) and total weights (W_{FINAL}) for the 5 rockfall susceptibility classes according to the Weights of Evidence Method, and the percentage of all rockfall features within each class

Susceptibility class	W+	W−	W_{FINAL}	Percentage of all rockfalls (%)
Very low	−3.0915	0.2265	−3.5141	0.96
Low	−2.6427	0.2165	−3.0553	1.47
Moderate	−1.4296	0.2352	−1.8609	6.19
High	0.4574	−0.2080	0.4689	38.59
Very High	1.8812	−0.6670	2.3518	52.79

Table 2 Positive (W+), negative (W−) and total weights (W_{FINAL}) for the 5 shallow landslide susceptibility classes according to the Weights of Evidence Method, and the percentage of all shallow landslide features within each class

Susceptibility Class	W+	W−	W_{FINAL}	Percentage of all landslides (%)
Very low	−2.9867	0.2921	−3.3472	1.49
Low	−1.3982	0.2215	−1.6881	6.55
Moderate	0.0782	−0.0270	0.0366	27.13
High	0.8031	−0.3410	1.0759	42.15
Very high	1.4843	−0.2140	1.6299	22.67

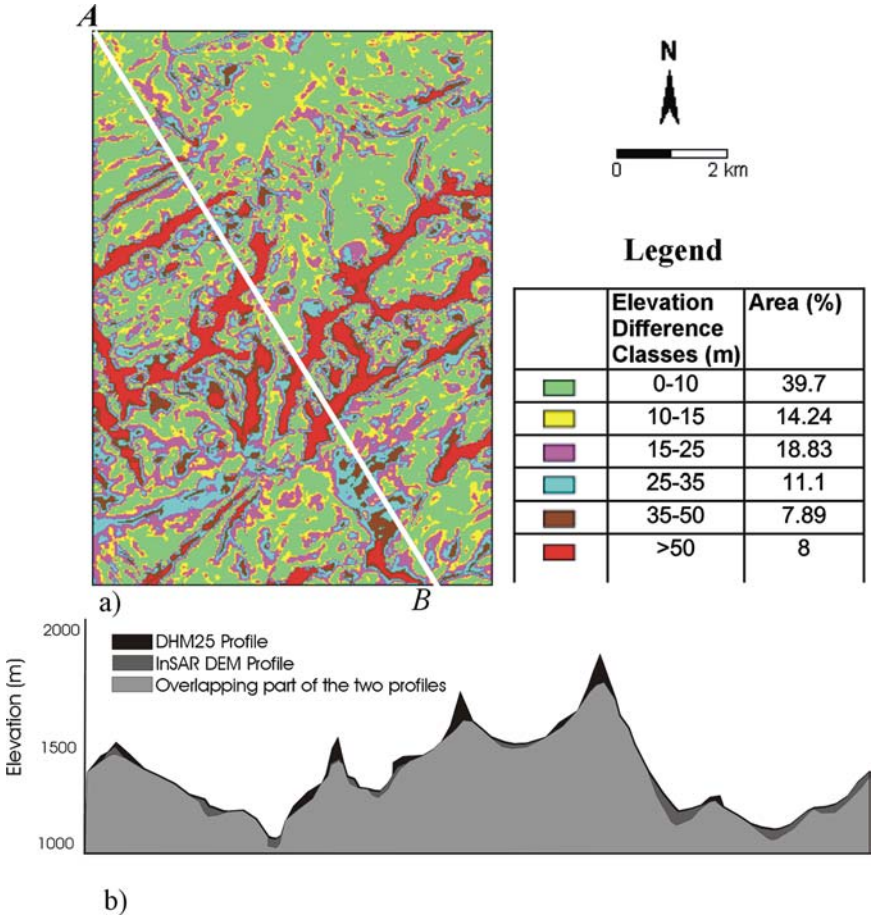

Fig. 4 Elevation difference between the DEMs derived from InSAR and from the Swiss topographic maps (DHM25); (**a**) Classified elevation difference map (DHM25—InSAR DEM). A–B is the line along which profile has been drawn below; (**b**) Elevation difference along profile A–B

areas are confined along the mountain ridges and valley bottoms. Part of this variation could be due to the fact that the generated InSAR-derived DEM corresponds to a Digital Surface Model, where height information in forested areas represents tree height, while DEMs obtained from digitized topographic maps (as the Swiss DHM25) must be regarded as Digital Terrain Models, where height information in forested areas represents terrain (ground) heights. This difference must also be considered while comparing the information contained in the two DEMs.

The error estimation was done for the absolute height as well as for slope steepness because for landslide susceptibility assessment slope steepness is a more important factor than absolute height. The two slope maps derived from the InSAR DEM and the DHM25 were compared in a GIS. The results are shown in Table 3.

From Table 3 it is evident that the InSAR derived DEM has a larger percentage of flatter slopes (0° to 20°) and a smaller percentage of slopes over 30°. A comparison of profiles drawn in each DEM across the general trend of ridges (for example along line A–B in Fig. 4) clearly reveals the differences in height and slope angle. It is evident that on the mountain ridges the InSAR DEM underestimates both the height and slope angles while along the valley sides it shows smaller slope angles and greater altitudes as compared to the DHM25. From these observations it can be concluded that the InSAR DEM smoothens the topography. The smoothening effect of the InSAR DEM is also demonstrated by the visual examination with 3-D perspective in anaglyph images created from the hill shading maps of DHM25 and InSAR DEM.

The effect of the error in altitude and slope on the landslide susceptibility mapping was evaluated by calculating landslide weights, using the Weights of Evidence method, for slope maps derived from the InSAR DEM and the DHM25, using the procedure described earlier (see Table 3). From the weight values of the slope classes for rockfalls as shown in Table 3 two trends can be inferred: (i) In the DHM25-derived slope map only the slopes steeper than 40° show positive weights for occurrence of rock fall whereas in the InSAR DEM-derived slope map the positive weights are observed right from slopes of 20° or steeper, which is not so realistic; (ii) In the InSAR derived slope map the weight values for all the slope classes are greater than those in corresponding slope classes of DHM25. Some of the areas, which are actually steeper, were wrongly included in the less steep classes due to the smoothening effect in the InSAR DEM as explained earlier and the positive weight of this class is due to the contribution from the more susceptible steeper areas, which are incorrectly included in this slope category. From these trends of weight values, it may be concluded that the susceptibility map derived from InSAR DEM-derived input maps is less reliable as it includes more areas with relatively gentle slopes as potentially susceptible to rockfall.

From the weight values for shallow landslides as shown in Table 3 it appears that the slope classes between 10–30° show a positive relationship in the DHM25-derived slope map indicating that gentle to moderate slopes are more susceptible to these type of mass movement. The comparison of weight values from the slope maps derived

Table 3 Comparison of slope classes in DHM25-derived and InSAR-derived slope maps and the weights of evidence for rockfall and shallow landslide features

Slope class (Degrees)	DHM25			InSAR DEM		
	Area (%)	Rockfall Weight	Shallow landslide Weight	Area (%)	Rockfall Weight	Shallow landslide Weight
<10	8.7	−2.78	−0.54	15.11	−1.08	−0.29
10–20	25.87	−2.82	0.94	37.57	−1.10	0.78
20–30	29	−2.14	0.27	31.2	0.16	−0.37
30–40	24.25	−0.55	−0.93	14.06	1.16	−1.63
40–50	8.45	1.66	−1.95	2.04	1.92	−3.74
>50	3.74	3.58	−3.98	0.03	4.11	−2.26

from DHM25 and InSAR indicates that both maps have a similar trend except for the 20–30° class. This class in the InSAR-derived slope map shows a negative relationship with the occurrence of landslides and thus contradicts with the weight value of DHM25 for the same slope class. Earlier it has been observed that for rockfall the same class in InSAR derived slope shows a positive weight. This observation further confirms that the majority of pixels in 20–30° slope class of InSAR derived slopes are in reality steeper slopes, which are less susceptible to shallow landslides.

Discussion and conclusions

This study shows that important terrain factors for landslide susceptibility analysis can be extracted from an InSAR DEM and through image classification of different combinations of multi temporal intensity images. The landslide susceptibility maps generated from the InSAR-derived input maps show good correlation with the original landslide inventory map. However, the accuracy of individual map classes is not always satisfactory. The comparison of the InSAR DEM with a DEM derived from a topographical map (DHM25) gives differences in height in the order of more than 50 m in high relief areas and in shadow zones in the valleys. The mean value of the difference is 20 m with a standard deviation of 21.5 m. Even though the altitude values derived from InSAR and DHM25 differ from each other because the former is a *Digital Surface Model* while the latter is a *Digital Terrain Model*, the deviation observed in the present case is too high to be caused only due to this reason. The comparison of profiles of InSAR DEM and DHM25 indicates that the InSAR underestimates the height at mountaintops while overestimating the lowest parts of the valleys. Platschorre (1997) states that this deviation is caused by the least square phase unwrapping. But in the present case a more sophisticated algorithm, which uses the fusion of a region growing and least square fit, has been applied and therefore the existence of these large errors on critical part of the slopes raise limitations of the InSAR-derived products for landslide susceptibility studies. It is because the slope class is a critical parameter for slope stability and any erroneous estimation of slope angles will have severe consequences for landslide susceptibility zonation, as was demonstrated by the values in Table 3.

The smoothening effect in InSAR DEM also limits the visual interpretation in 3-D perspective, e.g. using the anaglyph method, as the topographic details are blurred. As it has been observed in the profile, the smoothening effects are pronounced along the mountaintops and in the valleys. These are also the areas of low coherence due to layover and shadow. These low coherence areas are masked out before phase unwrapping (a coherence threshold is applied before unwrapping) and the phase values are interpolated and hence these are not the actual phase values. As a consequence, large height deviation compared with the reference DHM25 is noticed, especially along the areas of high relief.

Based on the above, it can be concluded that InSAR derived input maps are not ideal for landslide susceptibility assessment, but could be used if more accurate data is lacking. Currently the authors are evaluating a similar approach for landslide susceptibility mapping in part of the Indian Himalayas, where topographic data is restricted, and where InSAR derived data often is the only source of information available.

Acknowledgements

Part of this work was carried out in the framework of the DUP SLAM2 project "Service for Landslides Monitoring – Integration of Remote Sensing techniques with statistical methods for Landslide Monitoring and Risk Assessment" for the European Space Agency
We would like to thank Olivier Lateltin and Hugo Raetzo of the Swiss Federal Office for Water and Geology (FOWG) for providing us the landslide map of the study area, and Swisstopo for providing us the DHM25 Digital Elevation Model.

References

Antonello G, Casagli N, Farina P, Leva D, Nico G, Sieber AJ, Tarchi D (2004) Ground-based SAR interferometry for monitoring mass movements. Landslides 1(1):21–28

Bonham-Carter GF(1994) Geographic Information Systems for Geoscientists. Modelling with GIS. Computer Methods in the Geosciences. Pergamon 13:267–302

Colesanti C, Ferretti A, Prati C, Rocca F (2003) Monitoring landslides and tectonic motions with the permanent scatterers technique. Eng Geol 68(1–2):3–14

Chips (2000) http://www.geogr.ku.dk/chips/Manual/f167.htm

Crosetto M (2002) Calibration and validation of SAR interferometry for DEM generation. ISPRS J Photogram Remote Sens 57:213–227

De Grandi GF, Leysen M, Lee JS, Schuler D (1997) Radar reflective estimation using multiple SAR scenes of the same target: techniques and applications. Proceedings of IGARRS Conference, Singapore, pp 1047–1050

Fruneau B, Achache J, Delacourt C (1996) Observations and modeling of the Saint-Etiemme-de-Tinee landslide using SAR interferometry. Tectonophysics 265:181–190

Gens R, van Genderen JL (1996) SAR Interferometry – Issues, Techniques, Applications. Int J Remote Sens 17:1803–1835

Holecz F, Pasquali P, Moreira J, Meier E, Nüesch D (1998) Automatic Generation and Quality Assessment of Digital Surface Models generated from AeS-1 InSAR data. Proceedings of European Conference on Synthetic Aperture Radar, Friedrichshafen, Germany

Kimura H, Yamaguchi Y (2000) Detection of landslide areas using satellite radar interferometry. Photogram Eng Remote Sens 66(3):337–344

Massonnet D, Feigl KL (1998) Radar interferometry and its application to changes in the earth's surface. Rev Geophys 36(4):441–500

Pasquali P, Pellegrini R, Prati C, Rocca F (1994) Combination of interferograms from ascending and descending orbits. International Geosciences and Remote Sensing Symposium. Pasadena, CA, USA, pp 733–735

Pieraccini M, Casagli N, Luzi G, Tarchi D, Mecatti D, Noferini L, Atzeni C, (2003) Landslide monitoring by ground-based radar interferometry: A field test in Valdarno (Italy). Int J Remote Sens 24(6, 20):1385–1391

Platschorre Y (1997) A quantitative analysis of space borne derived elevation models. Unpublished M. Sc. Thesis, Delft University of Technology, 97 pp

Rabus B Eineder M, Roth A, Bamler R (2003) The shuttle radar topography mission–a new class of digital elevation models acquired by spaceborne radar. ISPRS J Photogram Remote Sens 57(4):241–262

Reigber A, Moreira J (1997) Phase unwrapping by fusion of local and global methods. Proceedings of IGARSS Symposium, Singapore

Rizo V, Tesauro M (2000) SAR interferometry and field data of Randazzo landslide (Eastern Sicily, Italy), Physics and Chemistry of the Earth, Part B: Hydrology. Oceans Atmos 25(9):771–780

Rosen PA, Hensley S, Joughin IR, Li FK, Madsen SN, Rodrıguez E, Goldstein RM, (2000) Synthetic aperture radar interferometry. Proce IEEE 88(3):333–382
Rott H, Scheuchl B, Siegel A, Grasemann B (1999) Monitoring very slow slope movements by means of SAR interferometry: a case study from a mass waste above a reservoir in the Ötztal Alps, Austria. Geophys Res Lett 26:1629–1632
Sarmap (2005) http://www.sarmap.ch/
Squarzoni C, Delacourt C, Allemand P (2003) Nine years of spatial and temporal evolution of the La Valette landslide observed by SAR interferometry. Eng Geol 68(1–2):53–66
Swisstopo (2002) http://www.swisstopo.ch/en/digital/dhm25.htm
Tarchi D, Casagli N, Moretti S, Leva D, Sieber AJ (2003) Monitoring landslide displacements by using ground-based synthetic aperture radar interferometry: Application to the Ruinon landslide in the Italian Alps. J Geophys Res B: Solid Earth 108(8):10–14
Van Westen CJ (1993) Application of Geographic Information Systems to Landslide Hazard Zonation. PhD Dissertation Technical University Delft. ITC Publication no. 15a, ITC, Enschede, the Netherlands, 245 pp

L. P. Singh
Geological Survey of India,
Hyderabad, India
e-mail: lalan_singh@alumni.itc.nl

C. J. van Westen (✉)
International Institute for Geo-Information Science and Earth Observation,
ITC, Enschede, The Netherlands
e-mail: westen@itc.nl
Tel.: +31-53-4874263
Fax: +31-53-4874336

P. K. Champati Ray
Indian Institute of Remote Sensing,
Dehradun, India
e-mail: champati_ray@iirs.gov.in

P. Pasquali
Sarmap, Cascine de Barico,
Purasca, Switzerland
e-mail: paolo.pasquali@sarmap.ch